海洋地质与第四纪地质
MARINE GEOLOGY & QUATERNARY GEOLOGY

岁差驱动的全新世热带太平洋—印度洋水汽输送

刘冰瑾，黄恩清，田　军

Precession forcing of the Holocene moisture transfer between tropical western Pacific and Indian Ocean

LIU Bingjin, HUANG Enqing, and TIAN Jun

在线阅读 View online: https://doi.org/10.16562/j.cnki.0256-1492.2023042001

您可能感兴趣的其他文章

Articles you may be interested in

西太平洋帕劳砗磲高分辨率氧同位素记录及其指示的气候环境变化

High-resolution oxygen isotope records of *Tridacna gigas* from Palau, Western Pacific and its climatic and environmental implications

海洋地质与第四纪地质. 2021, 41(1): 1

西太平洋-北印度洋及其洋陆过渡带：古今演变与论争

West Pacific and North Indian Oceans and Their Ocean-continent Connection Zones: Evolution and Debates

海洋地质与第四纪地质. 2017, 37(4): 1

南海南部上层水体浮游有孔虫的组成与分布特征

Assemblage and distribution of planktonic foraminifera in the upper water layer of southern South China Sea

海洋地质与第四纪地质. 2019, 39(1): 124

中全新世冲绳海槽北部的水文气候变化:浮游有孔虫群落证据

The hydroclimate changes in the northern Okinawa Trough during middle Holocene: Evidence from planktonic foraminiferal assemblages

海洋地质与第四纪地质. 2019, 39(1): 113

南海中部全新世以来海山深潜区有孔虫的地球化学记录及反映的气候变化

Geochemical record of foraminifera and its reflection on climate change in the central South China Sea since Holocene

海洋地质与第四纪地质. 2020, 40(2): 100

基于模型优化的广义自由表面多次波压制技术在印度洋深水海域的应用

Generalized free surface multiple suppression technique based on model optimization and its application to the deep water of the Indian Ocean

海洋地质与第四纪地质. 2021, 41(5): 221

ISSN 0256-1492 海洋地质与第四纪地质 第43卷第4期
CN 37-1117/P MARINE GEOLOGY & QUATERNARY GEOLOGY Vol.43, No.4

刘冰瑾, 黄恩清, 田军. 岁差驱动的全新世热带太平洋—印度洋水汽输送 [J]. 海洋地质与第四纪地质, 2023, 43(4): 56-70.
LIU Bingjin, HUANG Enqing, TIAN Jun. Precession forcing of the Holocene moisture transfer between tropical western Pacific and Indian Ocean[J]. Marine Geology & Quaternary Geology, 2023, 43(4): 56-70.

岁差驱动的全新世热带太平洋—印度洋水汽输送

刘冰瑾, 黄恩清, 田军
同济大学海洋地质国家重点实验室, 上海 200092

摘要: 大洋内部蒸发、水汽输送和降水过程构成了全球水文循环的主体, 但长久以来对全新世大洋内部水文循环的演变历史和驱动机制缺乏认识。利用全球热带海区98个站位混合层浮游有孔虫壳体的$\delta^{18}O$和Mg/Ca温度记录, 计算了全新世以来表层海水$\delta^{18}O$以及海水剩余$\delta^{18}O$的波动历史。发现最显著的特征是全新世以来热带西太平洋和东印度洋表层海水剩余$\delta^{18}O$具有不同的变化趋势。早—中全新世时期(11.5～6.0 kaBP), 热带西太平洋表层海水剩余$\delta^{18}O$比东印度洋偏重约0.2‰, 而晚全新世(2.0～0 kaBP), 两个海区的重建值几乎相同。结合同位素数值模拟结果, 发现岁差通过一系列机制控制了两个大洋不同的剩余$\delta^{18}O$变化信号。早全新世较低的岁差值可以驱动西太平洋往印度洋的大气水汽净输送并降低印度洋降水同位素, 同时强盛的南亚季风通过河流体系向孟加拉湾倾注了大量陆地冲淡水。这些机制都有利于东印度洋海水剩余$\delta^{18}O$出现相对负偏移信号。但较低的岁差值导致开放的西太平洋净降水量下降, 并通过大气传输损失淡水, 因此海水剩余$\delta^{18}O$值较为偏重。本次研究结合大空间尺度上的$\delta^{18}O$重建记录和模拟结果, 较为可靠地刻画了岁差调控下洋盆之间的水汽转移过程和机理。

关键词: 低纬水循环; 轨道周期; 海水氧同位素; 浮游有孔虫
中图分类号: P736 **文献标识码:** A **DOI:** 10.16562/j.cnki.0256-1492.2023042001

Precession forcing of the Holocene moisture transfer between tropical western Pacific and Indian Ocean

LIU Bingjin, HUANG Enqing, TIAN Jun
State Key Laboratory of Marine Geology, Tongji University, Shanghai 200092, China

Abstract: Precipitation, evaporation and moisture transport within the oceans are the main components of the global hydrological cycle. However, the evolution of the oceanic hydrological cycle over the Holocene remains a knowledge gap. In this study, through compiling paired planktonic foraminiferal $\delta^{18}O$ and Mg/Ca sea surface temperature reconstructions from 98 locations in the tropical ocean, we calculate the fluctuation of sea surface $\delta^{18}O$ and residual $\delta^{18}O$ for the Holocene period. We notice a striking feature that the residual $\delta^{18}O$ records of the tropical western Pacific and eastern Indian Ocean show a different change over the Holocene. The mean residual $\delta^{18}O$ of the tropical western Pacific was about 0.2‰ heavier than that of the eastern Indian Ocean during the early-mid Holocene (11.5～6.0 kaBP), but they were almost identical over the late Holocene (2.0～0 kaBP). Combined with the transient climate simulations, we suggest that precession forcing is responsible for this different pattern through modulating a set of climate processes. The lower precession over the early Holocene drove a net atmospheric moisture transport from the western Pacific to the eastern Indian Ocean and lowered precipitation $\delta^{18}O$ over the eastern Indian Ocean. Moreover, the strengthened South Asian monsoon delivered large amounts of diluted freshwater into the Bay of Bengal via river systems. All these three mechanisms contribute to a relatively negative excursion of residual $\delta^{18}O$ in the eastern Indian Ocean. In contrast, the lower precession resulted in a decrease of net precipitation in the open western Pacific and a loss of freshwater via the atmospheric transport, thus generating heavier residual $\delta^{18}O$ values. Through combining seawater $\delta^{18}O$ reconstructions from a large spatial extent with the isotope-enabled simulations, this study has provided a reliable picture of the moisture transfer between different ocean basins and unveiled the underlying mechanisms regulated by precession.

Key words: low-latitude hydrological cycle; orbital cycle; seawater oxygen isotope; planktonic foraminifera

---

资助项目: 国家自然科学基金优秀青年科学基金项目“低纬水循环地质演变”(42122042); 中央高校基本科研业务费专项资金项目“温室期低纬水文循环的地质演变”(22120220531)
作者简介: 刘冰瑾(1998—), 女, 硕士研究生, 海洋科学专业, E-mail: 2031672@tongji.edu.cn
通讯作者: 黄恩清(1984—), 男, 博士, 教授, 主要从事海洋地质研究, E-mail: ehuang@tongji.edu.cn
收稿日期: 2023-04-20; **改回日期:** 2023-05-26. 文凤英编辑

在传统描述中, 水文循环常常指的是水汽在大陆和大洋之间的循环, 但是大洋才是全球尺度上水文循环的主体。据估算, 大洋占了全球蒸发量的约 86% 和降水量的约 78%, 海洋蒸发量中仅约 10% 水汽输往大陆, 参与海陆间循环[1-2]。由于缺乏研究资料和手段, 海洋内部水文循环以及不同海盆之间水汽输送的地质演化历史基本还是认知上的空白。近年来, 随着表层海水氧同位素($\delta^{18}O_{sw}$)重建数据的增多以及同位素数值模式的应用, 对第四纪热带大洋内部水汽的输送变化获得了一些突破性认知。

首先, 晚第四纪表层海洋 $\delta^{18}O_{sw}$ 重建记录展现出显著的 10 万年左右的冰期-间冰期旋回周期, 说明高纬冰盖体积涨缩是控制 $\delta^{18}O_{sw}$ 波动的第一级要素[3]。这是因为冰盖氧同位素平均值约为–34‰, 大洋表层海水 $\delta^{18}O$ 平均值约为 0, 两个端元的同位素值差异巨大[4]。因此晚第四纪全球冰盖体积的巨大变化(可以引起全球海平面约 130 m 的升降)是全球海水 $\delta^{18}O$ 波动的主要来源[5]。其次, 通过间接方法可以估算出冰盖涨缩引起的海平面波动及其对海水同位素的影响效应(冰盖同位素效应)[6]。从表层海水 $\delta^{18}O_{sw}$ 信号中扣除掉该效应, 就可以获得剩余氧同位素值(residual $\delta^{18}O$, $\delta^{18}O_{resi}$)。海水 $\delta^{18}O_{resi}$ 受到多种因素影响, 包括洋面降水-蒸发平衡、降水 $\delta^{18}O$、陆地冲淡水输入、洋流混合等, 结合同位素数值模拟, 可以从 $\delta^{18}O_{resi}$ 波动记录中解读出重要的水文循环信息[7]。

通过对比晚第四纪全球各处的重建记录, 可以发现 $\delta^{18}O_{resi}$ 变化呈现出复杂的空间差异。在靠近陆地河口地区, $\delta^{18}O_{resi}$ 波动主要受到陆地冲淡水影响[8]。例如在非洲新几内亚湾, 海水 $\delta^{18}O_{resi}$ 呈现出显著的岁差周期, 并且与北半球夏至日太阳辐射量呈现同相位变化[9-10]。显然, 岁差调控的北非季风以及非洲赤道区河流径流量变化控制了 $\delta^{18}O_{resi}$ 信号。在赤道东太平洋、南海和冲绳海槽, $\delta^{18}O_{resi}$ 变化并没有明显的岁差周期[7, 11-12]。这些地区的 $\delta^{18}O_{resi}$ 信号可能受到多种气候过程的综合影响, 模糊了轨道驱动的印记[7]。最有趣的是, 在开放的热带西太平洋暖池地区, 数个站位高分辨率重建结果都显示 $\delta^{18}O_{resi}$ 变化中存在显著的岁差周期, 但与北半球夏至日太阳辐射量却呈现反相位变化[7, 13-14]。推测太阳辐射量高值期会引起洋面的强烈蒸发, 导致表层海水 $\delta^{18}O$ 值偏重[13]。

在同位素数值模拟结果中, 发现热带海区 $\delta^{18}O_{resi}$ 变化存在一个特别的空间分布特征, 即印度洋和西太平洋 $\delta^{18}O_{resi}$ 变化对岁差驱动的响应是相反的[13, 15]。在岁差低值期(即北半球太阳辐射量高值期), 热带西太平洋向印度洋的大气净水汽输送是增加的[13, 16], 这导致同时期的热带西太平洋 $\delta^{18}O_{resi}$ 偏重, 但印度洋 $\delta^{18}O_{resi}$ 偏轻, 两个大洋 $\delta^{18}O_{resi}$ 波动在岁差周期上存在反相位关系[13, 15]。如前所述, 这个模拟结果得到部分热带西太平洋重建数据的支持, 但还缺乏更大空间分布范围的证据, 特别是来自印度尼西亚多岛洋和印度洋地区的数据检验。因此, 本文通过收集全新世热带-亚热带海区(30ºS～30ºN)混合层浮游有孔虫壳体的氧同位素(planktonic foraminiferal $\delta^{18}O$, $\delta^{18}O_p$)和 Mg/Ca 温度(Mg/Ca-SST, sea surface temperature)记录, 计算 $\delta^{18}O_{sw}$ 和 $\delta^{18}O_{resi}$ 的演变历史。结合已经发表的模拟结果, 探索岁差对热带西太平洋—印度洋水汽输送的影响及其同位素表征。

1　材料与方法

1.1　数据来源与筛选标准

已发表的 $\delta^{18}O_p$ 和 Mg/Ca-SST 数据主要来自两个古海洋古环境学数据库: 德国不莱梅大学 PANGAEA 网站(https://www.pangaea.de/)和美国国家海洋和大气局 NOAA-paleo 数据集(https://www.ncei.noaa.gov/access/paleo-search/)。一部分数据没有收录于上述两个数据库, 散见于各类文献中。对数据的筛选标准如下: 首先, 为了严格限制重建结果为表层海水信息, 只选取生活于海洋混合层的浮游有孔虫数据, 热带亚热带海区的属种一般为 *Globigerinoides ruber* 和 *Globigerinoides sacculifer*。其次, 只选用 Mg/Ca-SST 数据, 排除了利用长链烯酮不饱和指数($U^{K'}_{37}$)和四醚膜类脂物(TEX_{86})指标获得的 SST 记录。在很多海区, Mg/Ca 与 $U^{K'}_{37}$ 指标倾向于记录不同季节的 SST 信息[12, 17-18], 而 TEX_{86} 指标很大程度上反映的是次表层海水温度变化[19]。$\delta^{18}O_p$ 和 Mg/Ca-SST 都来自浮游有孔虫这个信息载体, 可以更准确地重建 $\delta^{18}O_{sw}$。再次, 重建记录需要有良好的 AMS ^{14}C 定年数据进行年龄模式约束并具有较高的时间分辨率(＜200 年)。经过筛选, 共获得 98 个站位的重建数据, 其中低纬太平洋 52 个站位、印度洋 25 个站位、大西洋 21 个站位(图 1, 表 1)。

对原始数据进行如下处理: 首先, 国际工作组发表过不同版本的 ^{14}C 年龄与日历年龄的校正曲线, 最新版本为 IntCal20 以及专门用于海洋记录校正的 Marine20[20]。对于末次盛冰期以来的时段,

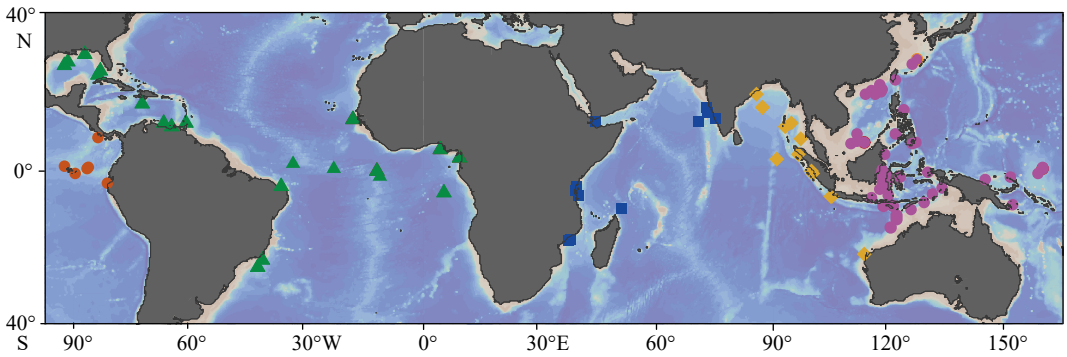

图 1 表层海水氧同位素重建数据的空间分布

站位点不同颜色和形状分别代表不同海洋区域。

Fig.1 Locations of reconstructed $\delta^{18}O_{sw}$ records in this study

Different colors and shapes of dots indicate records belonging to different ocean regions.

表 1 本文收集的海洋沉积站位信息

Table 1 Information of the stations of marine sedimentation used in this study

站位名称	站位位置	水深/m	种属	参考文献
A7	27.82°N、126.98°E	1 264	*G. ruber*	[21]
MD01-2404	26.65°N、125.81°E	1 397	*G. ruber*	[22-23]
MD01-2390	6.6°N、113.4°E	1 545	*G. ruber*	[24-25]
MD05-2896	8.83°N、111.44°E	1 657	*G. ruber*	[26]
MD05-2894	7.04°N、111.55°E	1982	*G. ruber*	[27]
CG2	6.39°N、110.15°E	1 239	*G. ruber*	[28-29]
MD05-2904	19.46°N、116.25°E	2 066	*G. ruber*	[30-31]
S0204B	20.23°N、118.05°E	1 533	*G. ruber*	[32]
MD97-2141	8.78°N、121.28°E	3 633	*G. ruber*	[33]
MD98-2178	3.62°N、118.7°E	1984	*G. ruber*	[34-35]
MD98-2161	5.21°S、117.48°E	1 185	*G. ruber*	[34-35]
MD06-3067	6.52°N、126.5°E	1 575	*G. ruber*	[36]
MD01-2386	1.13°S、129.79°E	2 816	*G. ruber*	[37]
GeoB17419-1/MD05-2920	2.81°S、144.5°E	1883	*G. ruber*	[38-39]
GeoB17426-3	2.19°S、150.86°E	1 368	*G. ruber*	[38-39]
KX973-22-4	0°N、159.23°E	2 362	*G. ruber*	[40]
KX973-21-2	1.42°S、157.98°E	1897	*G. ruber*	[41-42]
MD98-2176	5°S、133.44°E	2 382	*G. ruber*	[43-44]
MD98-2181	6.3°N、125.8°E	2 114	*G. ruber*	[45-46]
MD98-2188	14.82°N、123.49°E	730	*G. ruber*	[47]
70GGC	3.57°S、119.38°E	482	*G. ruber*	[48]
13GGC	7.4°S、115.2°E	594	*G. ruber*	[48]
SO217-18517	1.54°S、117.56°E	698	*G. ruber*	[49]
SO217-18515	3.63°S、119.36°E	688	*G. ruber*	[50]
SO217-18519	0.57°S、118.11°E	1 658	*G. ruber*	[51]

续表 1

站位名称	站位位置	水深/m	种属	参考文献
SO217-18522	1.4°S、119.08°E	975	*G. ruber*	[51]
SO217-18526	3.61°S、118.17°E	1 524	*G. ruber*	[51]
SO217-18540	6.87°S、119.58°E	1 189	*G. ruber*	[51]
SO217-18460	8.79°S、128.64°E	1875	*G. ruber*	[52]
MD98-2170	10.59°S、125.39°E	832	*G. ruber*	[45]
TR163-22	0.5°N、92.4°W	2 830	*G. ruber*	[53]
ODP1240	0.02°N、86.46°W	2 921	*G. ruber*	[54]
ME0005A-43JC	7.85°N、83.6°W	1 368	*G. ruber*	[55]
V21-30	1.2°S、89.7°W	617	*G. sacculifer*	[56]
ORI715-21	22.7°N、121.5°E	760	*G. ruber*	[57]
TGS-931	2.41°S、122.62°E	1912	*G. ruber*	[51]
ODP1242	7.85°N、83.6°W	1 364	*G. ruber*	[55]
ODP806b	0.32°N、159.36°E	2 520	*G. ruber*	[58]
ODP1145	19.58°N、117.63°E	3 175	*G. ruber*	[59]
GHE27L	19.85°N、115.34°E	1 533	*G. ruber*	[60]
GeoB16602	18.95°N、113.71°E	953	*G. ruber*	[61-62]
191PC	19.05°N、116.22°E	2 510	*G. ruber*	[63]
MD05-2905	21.36°N、117.36°E	1 647	*G. ruber*	[64]
M77/2-056-5	3.75°S、81.12°W	355	*G. ruber*	[65]
MD05-2925	9.34°S、151.46°E	1 661	*G. ruber*	[66]
SO18480-3	12.06°S、121.65°E	2 299	*G. ruber*	[13]
MD98-2162	4.69°S、117.9°E	1855	*G. ruber*	[13]
SO189-119KL	3.52°N、96.32°E	808	*G. ruber*	[67]
SO189-39KL	0.78°S、99.9°E	517	*G. ruber*	[67]
GeoB10029-4	1.49°S、100.13°E	964	*G. ruber*	[68]
GeoB10042-1	7.11°S、104.64°E	2 454	*G. ruber*	[69]
GeoB10043-3	7.31°S、105.06°E	2 171	*G. ruber*	[69]
MD98-2165	9.65°S、118.35°E	2 100	*G. ruber*	[70]
GeoB10069-3	9.6°S、120.9°E	1 250	*G. ruber*	[71]
MD01-2378	13.1°S、121.8°E	1 783	*G. ruber*	[72]
SO139-74KL	6.54°S、130.83°E	1 690	*G. ruber*	[73-74]
SK237-GC04	12.75°N、75°E	1 245	*G. ruber*	[75]
SK237-GC09	12.01°N、70.87°E	3 001	*G. ruber*	[76]
SK281/1	14.04°N、82°E	3 307	*G. ruber*	[77]
P178-15P	11.96°N、44.3°E	869	*G. ruber*	[78]
NGHP-01-17	10.75°N、93.11°E	1 356	*G. sacculifer*	[79]
ABP32GC01R	15.49°N、72.73°E	639	*G. sacculifer*	[80]

续表 1

站位名称	站位位置	水深/m	种属	参考文献
SK168/GC-1	11.71°N、94.49°E	2064	*G. sacculifer*	[81]
GeoB12610-2	4.82°S、39.42°E	399	*G. ruber*	[82]
GeoB12605-3	5.57°S、39.11°E	195	*G. ruber*	[83]
GeoB12615-4	7.14°S、39.84°E	446	*G. ruber*	[84]
GeoB16160-3	18.24°S、37.87°E	1339	*G. ruber*	[85]
AAS9_21	14.51°N、72.65°E	1807	*G. ruber*	[86]
WIND-28K	10.15°S、51.01°E	4157	*G. ruber*	[87]
GeoB9307-3/GeoB9310-4	18.57°S、37.38°E	542	*G. ruber*	[88]
U1446	19.08°N、85.74°E	1430	*G. ruber*	[89]
SO257-1-5	15.06°S、120.31°E	1608	*G. ruber*	[90]
SO257-5-9	22.11°S、113.49°E	1052	*G. ruber*	[90]
TR163-19	2.26°N、90.95°E	2348	*G. ruber*	[58]
ADM-C1	7.44°N、97°E	850	*G. ruber*	[91]
BoB-24	15.57°N、87.16°E	2769	*G. ruber*	[92]
MD02-2575	29°N、87.12°W	847	*G. ruber*	[93]
KNR166-2-26JPC	24.33°N、83.25°W	546	*G. ruber*	[94]
KNR159-JPC26	26.37°N、92.03°W	1995	*G. ruber*	[95]
EN32-PC6	26.95°N、91.35°W	2280	*G. ruber*	[96]
GeoB9526-5	12.44°N、18.06°W	3231	*G. ruber*	[97-98]
MD03-2707	2.5°N、9.39°E	1295	*G. ruber*	[10]
GeoB4905	2.5°N、9.39°E	1328	*G. ruber*	[99]
RC24-08	1.02°S、11.9°W	3882	*G. ruber*	[100]
SO164-03-4	16.54°N、72.21°W	2744.7	*G. ruber*	[101]
PL07-39PC	10.7°N、64.94°W	790	*G. ruber*	[102-103]
GeoB3129-3911	4.61°S、36.64°W	830	*G. ruber*	[104]
GL1090	24.92°S、42.51°W	2225	*G. ruber*	[105]
CF10-01B	23.6°S、41.6°W	130	*G. ruber white*	[106]
M78/1-235-1	11.61°N、60.96°W	852.2	*G. ruber*	[107]
VM12-107	11.33°N、66.63°W	1079	*G. ruber*	[108]
KNR166-2JPC51	24.41°N、83.22°W	198	*G. ruber white*	[108]
RC24-11	2.18°S、11.25°W	3445	*G. ruber white*	[100]
VM25-59	1.37°N、33.48°W	3824	*G. ruber white*	[100]
VM30-40	0.2°S、23.15°W	3706	*G. ruber white*	[100]
FAN17	4.81°N、4.45°E	1178	*G. ruber*	[109]
GeoB10038-4	5.94°S、5.25°E	1819	*G. ruber*	[68]

Marine13 之前的版本与之后的版本有较大差别，但 Marine13 与 20 版本结果非常接近。因此对于较老的重建记录，利用 Marine20 曲线对 AMS ^{14}C 定年结果进行重新校正并建立新的年龄模式。各个海区

的表层海洋碳储库效应(Δ*R*, 与全球热带海区平均碳储库年龄 405 a 的差值)一般依据原作者的估算, 如果缺乏该方面信息, 统一采用 0±200 a 的估算结果。其次, 不同海区浮游有孔虫壳体 Mg/Ca 比值与 SST 之间存在不同的经验换算公式, 本文接受原作者选择的公式, 保证重建的晚全新世平均 SST 结果(2～0 kaBP)与现代测量值一致。

1.2　重建表层和剩余海水氧同位素

根据实验室培养结果, 计算 $\delta^{18}O_{sw}$ 公式如下[110]:

$$\delta^{18}O_{sw}(‰, SMOW) = \delta^{18}O_p(‰, VPDB) + (SST - 16.5)/4.8 + 0.27 \quad (1)$$

需要指出的是, 该经验公式基于浮游有孔虫 *Orbulina universa* 的实验结果, 与本研究所利用的两种浮游有孔虫归于不同的属, 但该公式在热带大洋具有普适性[110-111]。进一步, 利用海平面与海水同位素换算关系来计算 $\delta^{18}O_{resi}$。末次盛冰期时全球海平面下降幅度 (Δ*h*) 约 130 m[112], 大洋海水 $\delta^{18}O$ 平均值增加约 1.0‰±0.1‰[113], 因此二者换算关系为 0.007 8‰±0.000 8‰/m。$\delta^{18}O_{resi}$ 计算公式为:

$$\delta^{18}O_{resi} = \delta^{18}O_{sw}(‰, SMOW) - 0.0078 \times \Delta h \quad (2)$$

考虑到 Mg/Ca-SST 温度估算(标准偏差为±1°C, ±1σ)以及公式 (1)、(2) 中各个系数的误差, $\delta^{18}O_{sw}$ 和 $\delta^{18}O_{resi}$ 估算的标准误差约为±0.3‰(±1σ)。

1.3　数据拟合方法

为了去除单个重建曲线包含的随机过程和噪音, 对 $\delta^{18}O_{sw}$、$\delta^{18}O_{resi}$ 重建结果进行区域和全球拟合($\delta^{18}O_{sw}$/$\delta^{18}O_{resi}$ stack)。参照前人发表成果[3, 12], 区域曲线的拟合方法如下: 每条曲线以 0.5 ka 为统计窗口, 对窗口内所有数据求平均值(每个窗口时间范围分别为 0.25～0.75 kaBP, 0.75～1.25 kaBP, …), 获得时间分辨率为 0.5 ka、数据等间距分布的曲线。再对每条曲线进行无权重平均, 获得区域拟合曲线。全球曲线的拟合方法与上述类似, 但为了避免各个区域 $\delta^{18}O_{sw}$ 绝对值差异对最终结果的影响, 先将每个站位 $\delta^{18}O_{sw}$ 曲线的平均值移动到零再进行拟合。按照曲线个数, 各个区域 $\delta^{18}O_{sw}$ 和 $\delta^{18}O_{resi}$ 拟合曲线的标准误差约为±0.04‰～0.12‰(±1σ, *n*=6—46)。全球 $\delta^{18}O_{sw}$ 拟合曲线的标准误差约为±0.03‰(±1σ, *n*=98)。

1.4　主成分分析

本文利用主成分分析 (principal component analysis, PCA) 提取不同区域 $\delta^{18}O_{sw}$ 重建序列的共同特征, 并利用 $\delta^{18}O_{sw}$ 曲线在主要成分上的载荷分布来分析 $\delta^{18}O_{sw}$ 变化的区域差异。部分站位 $\delta^{18}O_{sw}$ 数据较少或在时间序列上分布不均, 为了避免插值和外推带来的误差, 不纳入主成分分析。一共有 76 个站位的数据满足主成分分析要求。

1.5　海水同位素数值模拟

本文通过对比 $\delta^{18}O_{sw}$ 重建数据与同位素数值模拟结果, 试图解释热带大洋表层 $\delta^{18}O$ 变化机制及其背后的水文循环过程。同位素数值模拟来自先前发表结果[13]。瞬变模拟实验基于 GISS_ModelE2-R 海气耦合模型, 利用轨道参数和温室气体作为外强迫, 模拟了 30 万年来表层海水同位素和大气降水同位素的变化过程[13]。虽然这个实验缺乏动态冰盖模块, 不能评估冰盖变化对全球表层水同位素的影响, 但本次研究主要探究轨道驱动对大洋表层 $\delta^{18}O$ 的作用, 因此并不影响文章的主要结论。

2　结果

2.1　$\delta^{18}O_{sw}$ 拟合结果

如图 2 所示, 按照 $\delta^{18}O_{sw}$ 重建数据的绝对值分布范围, 我们将热带大洋划分为 5 个区域: 东印度洋(*n*=13)、西印度洋(*n*=12)、大西洋(*n*=21)、东太平洋(*n*=6)以及西太平洋(*n*=46), 分别做区域拟合, 在此基础上进一步做全球拟合(*n*=98)。11.5～0.5 kaBP 期间, 同一区域内不同站位的 $\delta^{18}O_{sw}$ 重建记录存在较大的绝对值差异, 东西印度洋、大西洋、东西太平洋的平均差异幅度分别为 1.09‰、1.23‰、2.37‰、0.78‰、1.32‰。不同区域 $\delta^{18}O_{sw}$ 拟合曲线的绝对值也存在差异, 可以分为两个部分, 其中西印度洋和大西洋的拟合结果比较接近, 而东西太平洋与东印度洋的拟合结果处在统一区间, 两部分之间的平均差异幅度约为 0.6‰。虽然存在绝对值差别, 但是 11.5 kaBP 以来各个区域拟合曲线持续变轻的振幅非常接近, 约为 0.8‰。相似的变化振幅暗示全新世热带 $\delta^{18}O_{sw}$ 变化受到同一因素控制。

考虑到不同海域 $\delta^{18}O_{sw}$ 存在的振幅差异, 将各个站位 $\delta^{18}O_{sw}$ 重建结果的平均值移动为零之后, 作全球拟合。如图 3 所示, 11.5～0.5 kaBP 期间, 全球 $\delta^{18}O_{sw}$ 拟合曲线持续负偏移, 与区域拟合曲线的变化趋势一致。不过全球拟合曲线的振幅约为 0.6‰, 比区域拟合数据的振幅小约 0.2‰。

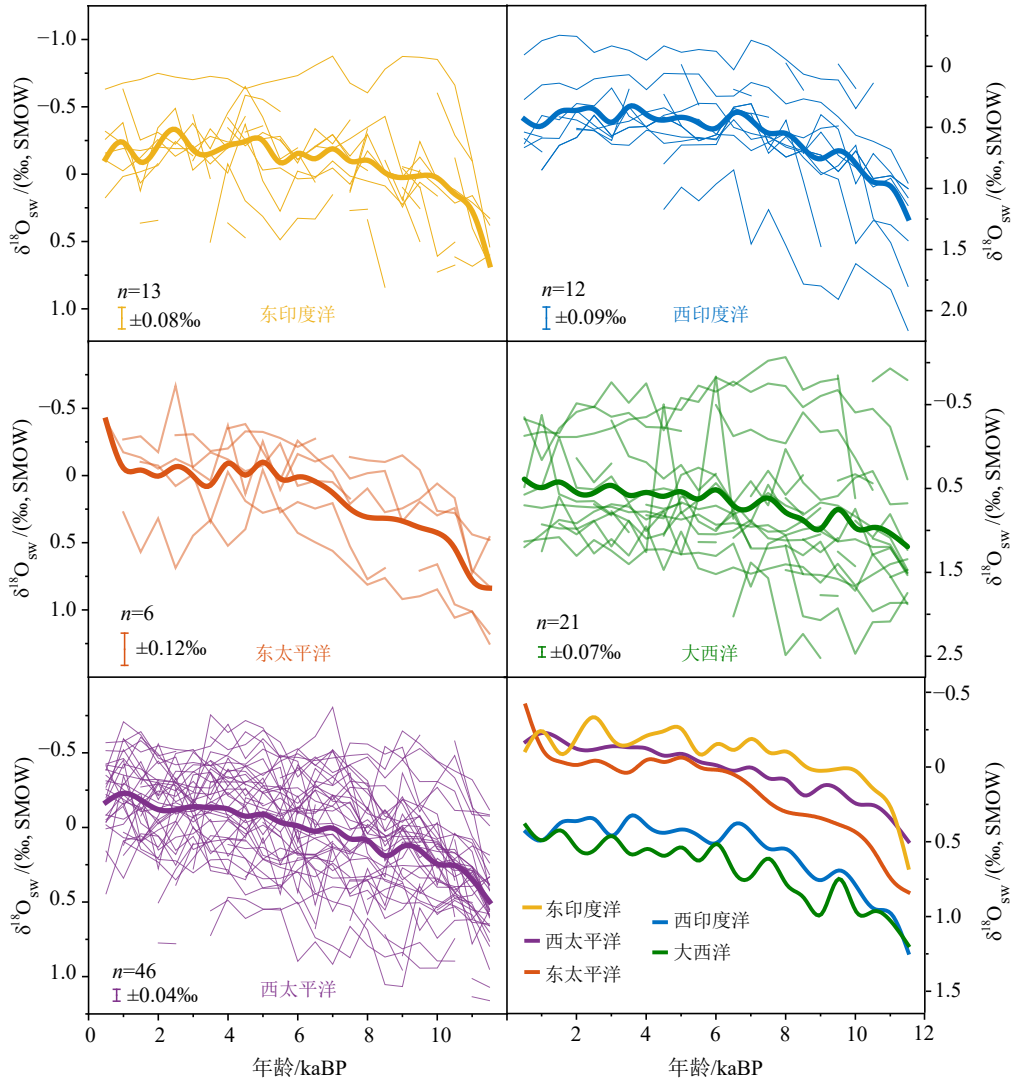

图 2 全新世各个热带大洋区域 $\delta^{18}O_{sw}$ 拟合曲线对比

图中标示了各条拟合曲线的标准误差 (±1σ)。

Fig.2 Comparison of the Holocene stacked $\delta^{18}O_{sw}$ records with those from different ocean regions

The standard error (±1σ) for each fitted curve is shown.

2.2 $\delta^{18}O_{sw}$ 主成分分析结果

对全球热带大洋 $\delta^{18}O_{sw}$ 时间序列进行主成分分析，只有 3 个成分的方差贡献率超过 5%，其中第一主成分（PC1）方差贡献率达 54.41%，其余两个成分方差贡献率分别为 8.93% 和 6.52%（表 2）。通过对比 11.5～0 kaBP 两条曲线的变化趋势，可以发现第一主成分主要代表全球 $\delta^{18}O_{sw}$ 拟合曲线在全新世持续负偏移的变化趋势（图 3）。在空间分布上，热带大洋绝大多数站位在第一主成分上的载荷也呈现一致变化（图 4）。除了大陆边缘的少数站位（南海北部、赤道非洲岸外、墨西哥湾和南美洲岸外），它们由于受到较强烈的陆地冲淡水影响，导致在第一主成分上的载荷接近零或者为负数。这些分析说明第一主成分代表了全球 $\delta^{18}O_{sw}$ 变化的最主要信息，并且指示第一主成分受到同一因素的控制。

2.3 西太平洋-东印度洋全新世 $\delta^{18}O_{resi}$ 变化的对比

从 $\delta^{18}O_{sw}$ 中扣除冰盖同位素效应的影响，可以获得 $\delta^{18}O_{resi}$。本文对比了早全新世（11.0～9.0 kaBP）、中全新世（7.0～5.0 kaBP）以及晚全新世（2.0～0 kaBP）3 个时间段 $\delta^{18}O_{resi}$ 在西太平洋-东印度洋的变化情形。如图 5 所示，相较于晚全新世，早全新世时西太平洋（南海除外）大部分站位（n=22，站位总数为 28）的重建 $\delta^{18}O_{resi}$ 值呈现正偏移，平均幅度为 0.15‰。半封闭的南海海盆情况较为复杂，靠陆架一侧站位显示负偏移信号，离开陆架的站位显示相反的正偏移信号。在东印度洋，孟加拉湾和苏门

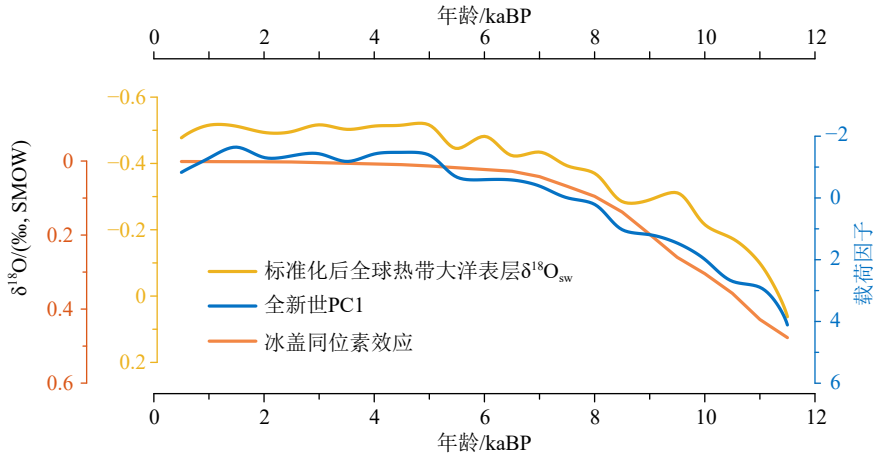

图 3　全新世 PC1、全球热带大洋表层 $\delta^{18}O_{sw}$ 拟合曲线与冰盖同位素效应的对比

冰盖 $\delta^{18}O$ 由海平面数据[112]计算得到。

Fig.3　Comparison of PC1, tropical surface ocean $\delta^{18}O_{sw}$ fitting and ice-volume isotope effect in the Holocene period

Ice-volume isotopic effect was calculated after reconstructed sea-level data[112].

表 2　全球热带大洋 $\delta^{18}O_{sw}$ 主成分分析结果

Table 2　Principal component analysis on $\delta^{18}O_{sw}$ of the global tropical ocean

成分	特征值	方差贡献率/%	方差累计贡献率/%
1	2.7472	54.41	54.41
2	0.4604	8.93	63.34
3	0.3128	6.52	69.87

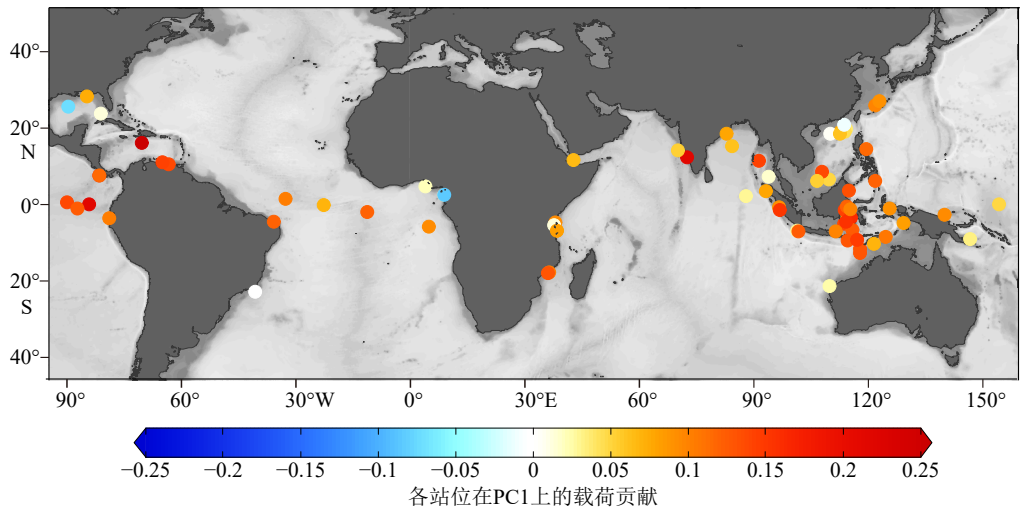

图 4　各站位在 PC1 成分上载荷贡献的空间分布

Fig.4　The spatial distribution of PC1 scores for each record

答腊岛岸外站位出现较为明显的负偏移信号, 其余站位呈现相对微弱的正偏移信号。

对比中、晚全新世两个时段的重建结果, 发现相比于晚全新世, 中全新世时西太平洋(南海除外)大部分站位(n=23, 站位总数为 29)$\delta^{18}O_{resi}$ 值仍然呈现显著的正偏移, 平均波动振幅为 0.13‰。南海海盆也重复同样的规律, 离开和靠近陆架的站位分别呈现正、负偏移信号。东印度洋情形发生变化, 绝大部分站位(n=8, 站位总数为 10)出现负偏移现象, 平均偏移幅度为 0.11‰。

全新世以来热带西太平洋(南海站位除外)和东印度洋 $\delta^{18}O_{resi}$ 不同变化趋势在区域拟合曲线中表现的尤为清楚。如图 6 所示, 11.5～6.0 kaBP 期间, 热带西太平洋 $\delta^{18}O_{resi}$ 平均值要比 2.0～0 kaBP

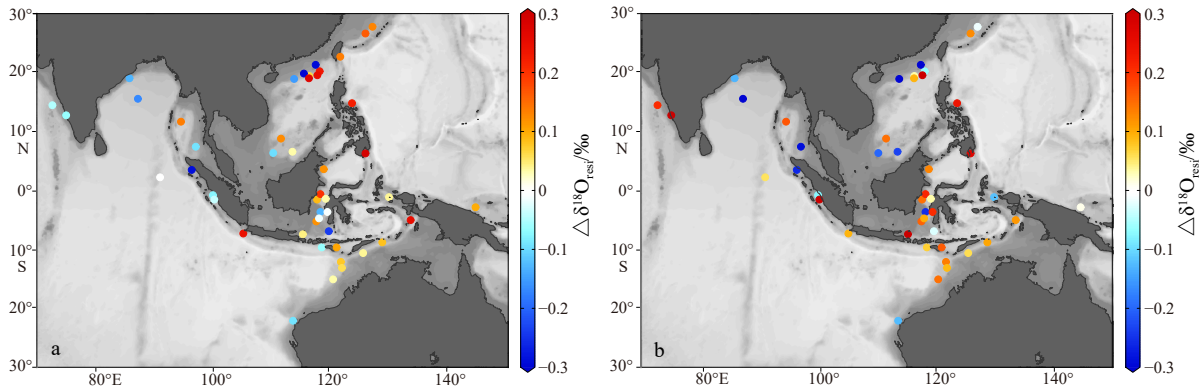

图 5 西太平洋-东印度洋不同时段 $\delta^{18}O_{resi}$ 差值（$\Delta\delta^{18}O_{resi}$）对比

a: 中全新世(7～5 kaBP)与晚全新世(2～0 kaBP)的 $\delta^{18}O_{resi}$ 差值, b: 早全新世(11～9 kaBP)和晚全新世的 $\delta^{18}O_{resi}$ 差值。

Fig.5 $\delta^{18}O_{resi}$ offsets of different time intervals across the Western Pacific-East Indian Ocean

a: $\delta^{18}O_{resi}$ offsets between the middle and the late Holocene, b: $\delta^{18}O_{resi}$ offsets between the early and the late Holocene.

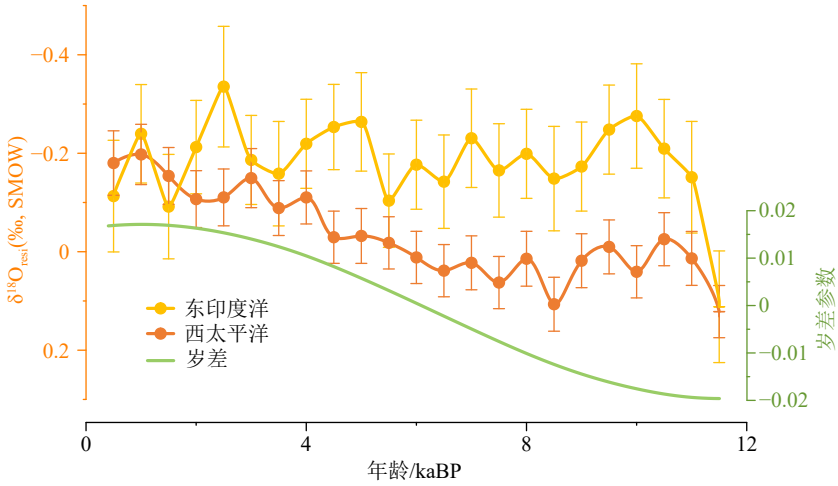

图 6 东印度洋、西太平洋 $\delta^{18}O_{resi}$ 拟合曲线与岁差参数的对比

其中, 西太平洋 $\delta^{18}O_{resi}$ 拟合曲线去除了南海区域的站位; 垂向误差线代表每个估算值的标准误差 (±1σ)。

Fig.6 Comparison of $\delta^{18}O_{resi}$ stacks for the Eastern Indian Ocean and the Western Pacific Ocean with precession

Reconstructions from the South China Sea are excluded from the Western Pacific $\delta^{18}O_{resi}$ stack. Vertical error bars indicate the standard error (±1σ) for each data point.

期间偏正约 0.15‰, 即全新世以来热带西太平洋表层 $\delta^{18}O_{resi}$ 整体发生了负偏移。相反, 东印度洋 $\delta^{18}O_{resi}$ 拟合曲线在 11.5～0 kaBP 期间发生了振幅约 0.2‰的数次波动, 但平均值变化幅度并不明显。对比这两条区域记录可以发现, 在早—中全新世(11.5～6.0 kaBP), 热带西太平洋 $\delta^{18}O_{resi}$ 比东印度洋要偏重 0.2‰, 但二者重建值在晚全新世时基本一致。

3 讨论

3.1 全新世不同热带海区 $\delta^{18}O_{sw}$ 绝对值差异的原因

在整个全新世, 大西洋 $\delta^{18}O_{sw}$ 拟合曲线比东太平洋重建结果总是偏重约 0.3‰～0.6‰(图 2)。这个区域差异在现代表层 $\delta^{18}O_{sw}$ 集成数据库中同样存在[114]。这是因为在东北信风的影响下, 在赤道巴拿马海道上空存在大西洋向太平洋的净水汽输送, 每年输送量约为 0.13～0.45 Sv[115-117](1 Sv 代表每秒一百万立方米), 并且在厄尔尼诺事件期间该水汽输送量更大[118]。由于北美科迪勒拉和南美安第斯山脉的影响, 太平洋水汽无法通过西风带传回大西洋, 这导致盐度和较重的 $\delta^{18}O$ 在大西洋亚热带地区持续累积[119]。另一个显著的区域差异存在于东西印度洋之间, 整个全新世西印度洋 $\delta^{18}O_{sw}$ 比东印度洋持续偏重约 0.65‰(图 2)。该特点同样反映在现代观测数据中, 但幅度较小, 仅为约 0.2‰[114]。印太

暖池区强烈的大气深对流运动导致东印度洋靠近东南亚一侧常年降水量偏高, 再加上南亚季风通过恒河和布拉马普特拉河向孟加拉湾倾泻了大量淡水, 导致东印度洋表层 $\delta^{18}O_{sw}$ 较低。而阿拉伯海位于副热带高压区, 蒸发量大于降水量, 且周边河流径流量较小, 因此表层盐度和 $\delta^{18}O_{sw}$ 高于孟加拉湾。总体上, 全新世 $\delta^{18}O_{sw}$ 拟合曲线准确再现了现代观测记录中不同热带海区表层海水同位素的差异。这说明重建的 $\delta^{18}O_{sw}$ 或者 $\delta^{18}O_{resi}$ 地质记录可以用来反映不同洋盆之间的水汽交换和水文循环的演变历史。

3.2　全新世热带大洋 $\delta^{18}O_{sw}$ 时间序列的变化原因

全球热带大洋 $\delta^{18}O_{sw}$ 拟合曲线可以去除随机噪音和各个站位的局部信号, 有利于辨别控制表层 $\delta^{18}O_{sw}$ 波动的主控因素。确实, 主成分分析(图 3, 图 4)也说明全新世以来热带大洋 $\delta^{18}O_{sw}$ 变化存在一个全球性的驱动因子。根据已发表的高精度重建数据, 11.5 kaBP 以来全球平均海平面上涨了约 63 m[112], 可以导致全球大洋 $\delta^{18}O$ 负偏移约 0.48‰(图 3, 公式 2)。因此推测海平面上涨是全新世热带大洋 $\delta^{18}O_{sw}$ 拟合曲线持续发生负偏移的主控因素。海平面上涨与热带大洋 $\delta^{18}O_{sw}$ 以及 PC1 变化速率也较为一致: 11.5～7.0 kaBP 期间二者速率较快, 对应于欧亚冰盖和北美劳伦泰冰盖的快速消融[120]; 7.0～5.0 kaBP 期间速率趋缓, 此时劳伦泰冰盖几乎完全消融[121], 但仍然有南极冰盖融冰水的贡献[122]; 5.0～0 kaBP 期间仅有微弱变化。

3.3　岁差驱动的热带太平洋-印度洋 $\delta^{18}O_{resi}$ 的差异性演变

由于 $\delta^{18}O_{resi}$ 结果中已经去除了全球冰盖同位素效应的影响, 因此各个区域 $\delta^{18}O_{resi}$ 拟合曲线可以指示不同洋盆海水同位素的差异化演变历史。在先前同位素模拟研究中, 已经发现全新世热带西太平洋与东印度洋表层 $\delta^{18}O_{resi}$ 的相反变化信号(图 7): 即相比于晚全新世, 早—中全新世西太平洋与东印度洋表层 $\delta^{18}O_{resi}$ 分别出现偏重和偏轻的信号[13, 15], 地质重建记录基本上支持这个同位素模拟结果, 但东印度洋一侧的部分研究站位出现了例外情形(图 5, 图 6)。可能受到局部过程的影响, 安达曼海(SK168/GC-1[81])、开放的印度洋(AAS9_21[86] 和 SK237/GC04[75])以及苏门答腊岛岸外(GeoB10043-3[69])4 个站位并没有显示出早—中全新世 $\delta^{18}O_{resi}$ 重建值比晚全新世更为负偏移的信号(图 5)。

全新世以来热带西太平洋与东印度洋表层海水 $\delta^{18}O_{resi}$ 记录的不同演变趋势应该是多个气候过程的综合结果。首先, 由于早—中全新世时岁差处于低值期, 拉尼娜气候态在热带太平洋地区占据主导地位[123-125]。印太暖池区温度升高, 导致大气深对流活动发育, 因此会给热带西太平洋和东印度洋陆地地区带来较多的降水和同位素值相对偏负的降水同位素[16, 126]。这个过程有利于靠近陆地边缘的海区出现表层海水 $\delta^{18}O_{resi}$ 负偏移的现象。但在开阔洋面, 包括南海南部和西太平洋, 反而出现降水减少的现象[13, 16, 89](图 7)。根据同位素数值模拟结

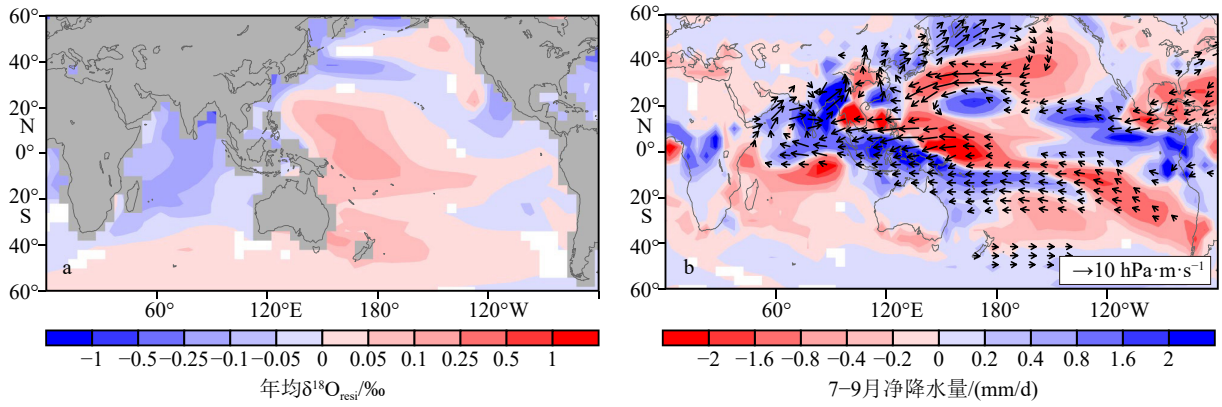

图 7　岁差驱动的热带表层海水 $\delta^{18}O_{resi}$ 和大气水汽输送变化

a: 模拟获得的热带表层海水年均 $\delta^{18}O_{resi}$ 在岁差极小值与极大值时期的差值, b: 模拟获得的 7—9 月期间净降水量以及大气水汽输送在岁差极小值与极大值时期的差值。模拟结果来自文献 [13]。

Fig.7　Precession forcing of changes in tropical sea surface $\delta^{18}O$ and atmospheric moisture transfer

a: Simulated tropical sea surface $\delta^{18}O_{resi}$ difference between precession minima and maxima, b: simulated changes in July-August-September net precipitation (precipitation minus evaporation) and atmospheric moisture transfer between precession minima and maxima. Simulation results are from Jian et al., 2022.

果，在岁差驱动下，存在热带西太平洋往印度洋的大气净水汽输送[13]，输送通道主要发生在南海南部到澳大利亚北部上空（17°S～18°N 区间，图 7b）。由于开阔的热带西太平洋洋面在岁差低值期存在净淡水损失，因此 $\delta^{18}O_{resi}$ 值反而出现正偏移现象。这个正偏移信号再通过洋流混合作用，导致整个西太平洋地区都出现显著的同位素正偏移信号（图 5，7）。

在东印度洋地区，除了接收来自西太平洋地区的大气水汽输入，早—中全新世较低的岁差值有利于大部分区域出现同位素较为偏负的降水[13-14]（图 7）。此外，南亚季风在早—中全新世强化，大量陆地冲淡水也进一步降低孟加拉湾海水的氧同位素值[89, 127]。孟加拉湾北部两个站位在早、中全新世显著的负偏移信号也证实了这一点（图 5）。但东印度洋地区降水变化的空间差异较大。一部分模型指出，相比于晚全新世，孟加拉湾北部、安达曼海以及苏门答腊岛西侧在早—中全新世时反而出现降水减少的现象[13-14, 89]（图 7）。这个过程与上述数个过程相反，会导致表层海水同位素的正偏移。正是多个气候过程的效果互相叠加，导致东印度洋 $\delta^{18}O_{resi}$ 拟合曲线在全新世没有呈现出明显的趋势变化。综上所述，岁差通过驱动多个气候过程，导致全新世西太平洋和东印度洋表层海水展现出不同的演化历史。

4 结论

(1) 全新世期间，不同海区 $\delta^{18}O_{sw}$ 拟合曲线存在较为明显的绝对值差异，表现为大西洋 $\delta^{18}O_{sw}$ 拟合曲线比同纬度的太平洋偏重，西印度洋 $\delta^{18}O_{sw}$ 拟合曲线比东印度洋偏重。该差异与现代观测结果一致。由于赤道信风的影响，大西洋通过中美洲上空的大气水汽输送持续向太平洋输入淡水，因此同位素值偏重。东印度洋较轻的 $\delta^{18}O_{sw}$ 值主要受到南亚季风带来的陆地冲淡水的影响。全新世以来全球热带大洋 $\delta^{18}O_{sw}$ 拟合曲线都表现出持续变轻的趋势，偏移振幅约为 0.6‰。主成分分析表明这个负偏移信号是绝大部分站位的共有特征，推测全新世以来冰盖消融和全球海平面上涨是导致这个变化的主要原因，冰盖同位素效应可以导致表层海水 $\delta^{18}O_{sw}$ 偏轻约 0.5‰。

(2) 重建记录和模拟都证实，全新世以来热带西太平洋与东印度洋表层海水 $\delta^{18}O_{resi}$ 发生了不同变化。岁差通过调控跨洋盆的大气水汽输送、降水同位素和陆地冲淡水规模，导致早—中全新世热带西太平洋表层海水 $\delta^{18}O_{resi}$ 值比东印度洋相对更加偏重。

参考文献 (References)

[1] Trenberth K E, Fasullo J T, Mackaro J. Atmospheric moisture transports from ocean to land and global energy flows in reanalyses [J]. Journal of Climate, 2011, 24(18): 4907-4924.

[2] Gimeno L, Stohl A, Trigo R M, et al. Oceanic and terrestrial sources of continental precipitation [J]. Reviews of Geophysics, 2012, 50(4): RG4003.

[3] Shakun J D, Lea D W, Lisiecki L E, et al. An 800-kyr record of global surface ocean δ^{18} O and implications for ice volume-temperature coupling [J]. Earth and Planetary Science Letters, 2015, 426: 58-68.

[4] Coplen T B, Herczeg A L, Barnes C. Isotope engineering—using stable isotopes of the water molecule to solve practical problems [J]. Environmental tracers in subsurface hydrology, 2000: 79-110.

[5] Shackleton N J. Attainment of isotopic equilibrium between ocean water and the benthonic foraminifera genus *Uvigerina*: isotopic changes in the ocean during the last glacial[C]//Proceedings of the Colloques Internationaux du C. N. R. S. 1974.

[6] Zhang P, Xu J, Holbourn A, et al. Obliquity induced latitudinal migration of the Intertropical Convergence Zone during the past~ 410 kyr [J]. Geophysical Research Letters, 2022, 49(21): e2022GL100039.

[7] 黄恩清, 赵蔓, 王跃, 等. 第四纪热带西太平洋表层海水氧同位素的岁差周期[J]. 第四纪研究, 2020, 40(6)：1464-1473. [HUANG Enqing, ZHAO Man, WANG Yue, et al. Quaternary precession cycles of sea-surface oxygen isotope records from the tropical western Pacific [J]. Quaternary Sciences, 2020, 40(6): 1464-1473.]

[8] Zhang P, Xu J, Beil S, et al. Variability in Indonesian throughflow upper hydrology in response to precession‐induced tropical climate processes over the past 120 kyr [J]. Journal of Geophysical Research: Oceans, 2021, 126(8): e2020JC017014.

[9] Weldeab S. Bipolar modulation of millennial-scale West African monsoon variability during the last glacial (75, 000–25, 000 years ago) [J]. Quaternary Science Reviews, 2012, 40: 21-29.

[10] Weldeab S, Lea D W, Schneider R R, et al. 155, 000 years of West African monsoon and ocean thermal evolution [J]. Science, 2007, 316(5829): 1303-1307.

[11] Clemens S C, Holbourn A, Kubota Y, et al. Precession-band variance missing from East Asian monsoon runoff [J]. Nature Communications, 2018, 9(1): 3364.

[12] Huang E Q, Wang P X, Wang Y, et al. Dole effect as a measurement of the low-latitude hydrological cycle over the past 800 ka [J]. Science Advances, 2020, 6(41): eaba4823.

[13] Jian Z M, Wang Y, Dang H W, et al. Warm pool ocean heat content regulates ocean–continent moisture transport [J]. Nature, 2022, 612(7938): 92-99.

[14] Cheng H, Li H Y, Sha L J, et al. Milankovitch theory and monsoon [J]. The Innovation, 2022, 3(6): 100338.

[15] Schmidt G A, LeGrande A N, Hoffmann G. Water isotope expressions of intrinsic and forced variability in a coupled ocean‐atmosphere model [J]. Journal of Geophysical Research:Atmospheres, 2007, 112(D10): D10103.

[16] 石正国, 雷婧, 周朋, 等. 轨道尺度亚洲气候演化机理的数值模拟:

历史与展望[J]. 第四纪研究, 2020, 40(1): 8-17. [SHI Zhengguo, LEI Jing, ZHOU Peng, et al. Numerical simulation researches on orbital-scale Asian climate dynamics: history and perspective [J]. Quaternary Sciences, 2020, 40(1): 8-17.]

[17] Leduc G, Schneider R, Kim J H, et al. Holocene and Eemian sea surface temperature trends as revealed by alkenone and Mg/Ca paleothermometry [J]. Quaternary Science Reviews, 2010, 29(7-8): 989-1004.

[18] Huang E Q, Tian J, Steinke S. Millennial-scale dynamics of the winter cold tongue in the southern South China Sea over the past 26 ka and the East Asian winter monsoon [J]. Quaternary Research, 2011, 75(1): 196-204.

[19] Tierney J E, Tingley M P. A TEX_{86} surface sediment database and extended Bayesian calibration [J]. Scientific Data, 2015, 2: 150029.

[20] Heaton T J, Bard E, Bronk Ramsey C, et al. Radiocarbon: a key tracer for studying Earth's dynamo, climate system, carbon cycle, and Sun [J]. Science, 2021, 374(6568): eabd7096.

[21] Sun Y B, Oppo D W, Xiang R, et al. Last deglaciation in the Okinawa Trough: subtropical northwest Pacific link to Northern Hemisphere and tropical climate [J]. Paleoceanography, 2005, 20(4): PA4005.

[22] Chang Y P, Chen M T, Yokoyama Y, et al. Monsoon hydrography and productivity changes in the East China Sea during the past 100, 000 years: okinawa Trough evidence (MD012404) [J]. Paleoceanography, 2009, 24(3): PA3208.

[23] Chen M T, Lin X P, Chang Y P, et al. Dynamic millennial - scale climate changes in the northwestern Pacific over the past 40, 000 years [J]. Geophysical Research Letters, 2010, 37(23): L23603.

[24] Steinke S, Kienast M, Groeneveld J, et al. Proxy dependence of the temporal pattern of deglacial warming in the tropical South China Sea: toward resolving seasonality [J]. Quaternary Science Reviews, 2008, 27(7-8): 688-700.

[25] Steinke S, Mohtadi M, Groeneveld J, et al. Reconstructing the southern South China Sea upper water column structure since the Last Glacial Maximum: implications for the East Asian winter monsoon development [J]. Paleoceanography, 2010, 25(2): PA2219.

[26] Tian J, Huang E Q, Pak D K. East Asian winter monsoon variability over the last glacial cycle: insights from a latitudinal sea-surface temperature gradient across the South China Sea [J]. Palaeogeography, Palaeoclimatology, Palaeoecology, 2010, 292(1-2): 319-324.

[27] An Y, Jian Z M. *Pulleniatina* Minimum Event during the last deglaciation in the southern South China Sea [J]. Chinese Science Bulletin, 2009, 54(23): 4514-4519.

[28] 郝鹏, 李铁刚, 常凤鸣, 等. 末次盛冰期以来南海西南海区对快速气候变化的响应特征[J]. 海洋地质与第四纪地质, 2014, 34(4): 83-91. [HAO Peng, LI Tiegang, CHANG Fengming, et al. Response of the southwestern South China Sea to the rapid climate changes since the last glacial maximum [J]. Marine Geology & Quaternary Geology, 2014, 34(4): 83-91.]

[29] Huang J, Wan S M, Li A C, et al. Two-phase structure of tropical hydroclimate during Heinrich Stadial 1 and its global implications [J]. Quaternary Science Reviews, 2019, 222: 105900.

[30] 葛黄敏, 李前裕, 成鑫荣, 等. 南海北部晚第四纪高分辨率浮游氧同位素地层学及其古气候信息[J]. 地球科学-中国地质大学学报, 2010, 35(4): 515-525. [GE Huangmin, LI Qianyu, CHENG Xinrong, et al. Late Quaternary high resolution monsoon records in planktonic stable isotopes from northern South China Sea [J]. Earth Science-Journal of China University of Geosciences, 2010, 35(4): 515-525.]

[31] Wang P X, Li Q Y, Tian J, et al. Monsoon influence on planktic $\delta^{18}O$ records from the South China Sea [J]. Quaternary Science Reviews, 2016, 142: 26-39.

[32] Yang Y P, Xiang R, Zhang L L, et al. Is the upward release of intermediate ocean heat content a possible engine for low-latitude processes? [J]. Geology, 2020, 48(6): 579-583.

[33] Rosenthal Y, Oppo D W, Linsley B K. The amplitude and phasing of climate change during the last deglaciation in the Sulu Sea, western equatorial Pacific [J]. Geophysical Research Letters, 2003, 30(8): 1428.

[34] Fan W J, Jian Z M, Bassinot F, et al. Holocene centennial-scale changes of the Indonesian and South China Sea throughflows: evidences from the Makassar Strait [J]. Global and Planetary Change, 2013, 111: 111-117.

[35] Fan W J, Jian Z M, Chu Z H, et al. Variability of the Indonesian throughflow in the Makassar Strait over the last 30 ka [J]. Scientific Reports, 2018, 8(1): 5678.

[36] Bolliet T, Holbourn A, Kuhnt W, et al. Mindanao Dome variability over the last 160 kyr: episodic glacial cooling of the West Pacific Warm Pool [J]. Paleoceanography, 2011, 26(1): PA1208.

[37] Jian Z M, Wang Y, Dang H W, et al. Half-precessional cycle of thermocline temperature in the western equatorial Pacific and its bihemispheric dynamics [J]. Proceedings of the National Academy of Sciences of the United States of America, 2020, 117(13): 7044-7051.

[38] Hollstein M, Mohtadi M, Rosenthal Y, et al. Variations in Western Pacific Warm Pool surface and thermocline conditions over the past 110, 000 years: forcing mechanisms and implications for the glacial Walker circulation [J]. Quaternary Science Reviews, 2018, 201: 429-445.

[39] Tachikawa K, Timmermann A, Vidal L, et al. CO_2 radiative forcing and Intertropical Convergence Zone influences on western Pacific warm pool climate over the past 400 ka [J]. Quaternary Science Reviews, 2014, 86: 24-34.

[40] Hollstein M, Mohtadi M, Kienast M, et al. The impact of astronomical forcing on surface and thermocline variability within the Western Pacific Warm Pool over the past 160 kyr [J]. Paleoceanography and Paleoclimatology, 2020, 35(6): e2019PA003832.

[41] Zhang S, Li T G, Chang F M, et al. Correspondence between the ENSO-like state and glacial-interglacial condition during the past 360 kyr [J]. Chinese Journal of Oceanology and Limnology, 2017, 35(5): 1018-1031.

[42] Zhang S, Yu Z F, Wang Y, et al. Thermal coupling of the Indo-Pacific warm pool and Southern Ocean over the past 30, 000 years [J]. Nature Communications, 2022, 13(1): 5457.

[43] Dang H W, Jian Z M, Wang Y, et al. Pacific warm pool subsurface

heat sequestration modulated Walker circulation and ENSO activity during the Holocene [J]. Science Advances, 2020, 6(42): eabc0402.

[44] Dang H W, Wu J W, Xiong Z F, et al. Orbital and sea-level changes regulate the iron-associated sediment supplies from Papua New Guinea to the equatorial Pacific [J]. Quaternary Science Reviews, 2020, 239: 106361.

[45] Stott L D. Comment on "Anomalous radiocarbon ages for foraminifera shells" by W. Broecker et al. : a correction to the western tropical Pacific MD9821-81 record [J]. Paleoceanography, 2007, 22(1): PA1211.

[46] Saikku R, Stott L, Thunell R. A bi-polar signal recorded in the western tropical Pacific: northern and Southern Hemisphere climate records from the Pacific warm pool during the last Ice Age [J]. Quaternary Science Reviews, 2009, 28(23-24): 2374-2385.

[47] Dang H W, Jian Z M, Bassinot F, et al. Decoupled Holocene variability in surface and thermocline water temperatures of the Indo‐Pacific Warm Pool [J]. Geophysical Research Letters, 2012, 39(1): L01701.

[48] Linsley B K, Rosenthal Y, Oppo D W. Holocene evolution of the Indonesian throughflow and the western Pacific warm pool [J]. Nature Geoscience, 2010, 3(8): 578-583.

[49] Hendrizan M, Kuhnt W, Holbourn A. Variability of indonesian throughflow and borneo runoff during the last 14 kyr [J]. Paleoceanography, 2017, 32(10): 1054-1069.

[50] Schröder J F, Holbourn A, Kuhnt W, et al. Variations in sea surface hydrology in the southern Makassar Strait over the past 26 kyr [J]. Quaternary Science Reviews, 2016, 154: 143-156.

[51] Schröder J F, Kuhnt W, Holbourn A, et al. Deglacial warming and hydroclimate variability in the central Indonesian Archipelago [J]. Paleoceanography and Paleoclimatology, 2018, 33(9): 974-993.

[52] 张鹏, 徐建, 杨策, 等. 末次冰期以来印尼穿越流出口处古海洋学记录及其意义[J]. 海洋地质与第四纪地质, 2017, 37(3): 129-137. [ZHANG Peng, XU Jian, YANG Ce, et al. Paleoceanographic records of Indonesian throughflow at its exit since the last glacial and their significance [J]. Marine Geology & Quaternary Geology, 2017, 37(3): 129-137.]

[53] Lea D W, Pak D K, Belanger C L, et al. Paleoclimate history of Galápagos surface waters over the last 135, 000 yr [J]. Quaternary Science Reviews, 2006, 25(11-12): 1152-1167.

[54] Pena L D, Cacho I, Ferretti P, et al. El Niño–Southern Oscillation–like variability during glacial terminations and interlatitudinal teleconnections [J]. Paleoceanography, 2008, 23(3): PA3101.

[55] Benway H M, Mix A C, Haley B A, et al. Eastern Pacific Warm Pool paleosalinity and climate variability: 0–30 kyr [J]. Paleoceanography, 2006, 21(3): PA3008.

[56] Koutavas A, Lynch-Stieglitz J, Marchitto Jr T M, et al. El Niño-like pattern in ice age tropical Pacific sea surface temperature [J]. Science, 2002, 297(5579): 226-230.

[57] Lo L, Lai Y H, Wei K Y, et al. Persistent sea surface temperature and declined sea surface salinity in the northwestern tropical Pacific over the past 7500 years [J]. Journal of Asian Earth Sciences, 2013, 66: 234-239.

[58] Lea D W, Pak D K, Spero H J. Climate impact of late quaternary equatorial pacific sea surface temperature variations [J]. Science, 2000, 289(5485): 1719-1724.

[59] Oppo D W, Sun Y B. Amplitude and timing of sea-surface temperature change in the northern South China Sea: dynamic link to the East Asian monsoon [J]. Geology, 2005, 33(10): 785-788.

[60] Yang Y P, Xiang R, Liu J G, et al. Inconsistent sea surface temperature and salinity changing trend in the northern South China Sea since 7.0 ka BP [J]. Journal of Asian Earth Sciences, 2019, 171: 178-186.

[61] Cheng Z J, Weng C Y, Steinke S, et al. Anthropogenic modification of vegetated landscapes in southern China from 6, 000 years ago [J]. Nature Geoscience, 2018, 11(12): 939-943.

[62] Huang E Q, Chen Y R, Schefuß E, et al. Precession and glacial-cycle controls of monsoon precipitation isotope changes over East Asia during the Pleistocene [J]. Earth and Planetary Science Letters, 2018, 494: 1-11.

[63] 范维佳, 陈荣华. 南海北部5万年来的表层海水盐度及东亚季风降水[J]. 第四纪研究, 2011, 31(2): 227-235. [FAN Weijia, CHEN Ronghua. Sea surface salinity and East Asian monsoon precipitation since the last 50000 years in the northern South China Sea [J]. Quaternary Sciences, 2011, 31(2): 227-235.]

[64] 杨文光, 郑洪波, 王可, 等. 南海东北部MD05-2905站36ka BP以来的陆源碎屑沉积特征与东亚季风的演化[J]. 地球科学进展, 2007, 22(10): 1012-1018. [YANG W G, ZHENG H B, WANG K, et al. Sedimentary characteristic of terrigenous clast of site MD05-2905 in the northeastern part of South China Sea after 36ka and evolution of East Asian monsoon [J]. Advances in Earth Science, 2007, 22(10): 1012-1018.]

[65] Nürnberg D, Böschen T, Doering K, et al. Sea surface and subsurface circulation dynamics off equatorial Peru during the last ~ 17 kyr [J]. Paleoceanography, 2015, 30(7): 984-999.

[66] Lo L, Chang S P, Wei K Y, et al. Nonlinear climatic sensitivity to greenhouse gases over past 4 glacial/interglacial cycles [J]. Scientific Reports, 2017, 7(1): 4626.

[67] Mohtadi M, Prange M, Oppo D W, et al. North Atlantic forcing of tropical Indian Ocean climate [J]. Nature, 2014, 509(7498): 76-80.

[68] Mohtadi M, Steinke S, Lückge A, et al. Glacial to Holocene surface hydrography of the tropical eastern Indian Ocean [J]. Earth and Planetary Science Letters, 2010, 292(1-2): 89-97.

[69] Setiawan R Y, Mohtadi M, Southon J, et al. The consequences of opening the Sunda Strait on the hydrography of the eastern tropical Indian Ocean [J]. Paleoceanography, 2015, 30(10): 1358-1372.

[70] Levi C, Labeyrie L, Bassinot F, et al. Low‐latitude hydrological cycle and rapid climate changes during the last deglaciation [J]. Geochemistry, Geophysics, Geosystems, 2007, 8(5): Q05N12.

[71] Gibbons F T, Oppo D W, Mohtadi M, et al. Deglacial $\delta^{18}O$ and hydrologic variability in the tropical Pacific and Indian Oceans [J]. Earth and Planetary Science Letters, 2014, 387: 240-251.

[72] Xu J, Holbourn A, Kuhnt W, et al. Changes in the thermocline structure of the Indonesian outflow during Terminations I and II [J]. Earth and Planetary Science Letters, 2008, 273(1-2): 152-162.

[73] Lückge A, Mohtadi M, Rühlemann C, et al. Monsoon versus ocean

circulation controls on paleoenvironmental conditions off southern Sumatra during the past 300, 000 years [J]. Paleoceanography, 2009, 24(1): PA1208.

[74] Wang X X, Jian Z M, Lückge A, et al. Precession-paced thermocline water temperature changes in response to upwelling conditions off southern Sumatra over the past 300, 000 years [J]. Quaternary Science Reviews, 2018, 192: 123-134.

[75] Saraswat R, Lea D W, Nigam R, et al. Deglaciation in the tropical Indian Ocean driven by interplay between the regional monsoon and global teleconnections [J]. Earth and Planetary Science Letters, 2013, 375: 166-175.

[76] Saraswat R, Singh D P, Lea D W, et al. Indonesian throughflow controlled the westward extent of the Indo-Pacific Warm Pool during glacial-interglacial intervals [J]. Global and Planetary Change, 2019, 183: 103031.

[77] Govil P, Naidu P D. Variations of Indian monsoon precipitation during the last 32 kyr reflected in the surface hydrography of the Western Bay of Bengal [J]. Quaternary Science Reviews, 2011, 30(27-28): 3871-3879.

[78] Tierney J E, Pausata F S R, deMenocal P. Deglacial Indian monsoon failure and North Atlantic stadials linked by Indian Ocean surface cooling [J]. Nature Geoscience, 2016, 9(1): 46-50.

[79] Gebregiorgis D, Hathorne E C, Giosan L, et al. Southern Hemisphere forcing of South Asian monsoon precipitation over the past~ 1 million years [J]. Nature Communications, 2018, 9(1): 4702.

[80] Banakar V K, Baidya S, Piotrowski A M, et al. Indian summer monsoon forcing on the deglacial polar cold reversals [J]. Journal of Earth System Science, 2017, 126(6): 87.

[81] Gebregiorgis D, Hathorne E C, Sijinkumar A V, et al. South Asian summer monsoon variability during the last ~54 kyrs inferred from surface water salinity and river runoff proxies [J]. Quaternary Science Reviews, 2016, 138: 6-15.

[82] Rippert N, Baumann K H, Pätzold J. Thermocline fluctuations in the western tropical Indian Ocean during the past 35 ka [J]. Journal of Quaternary Science, 2015, 30(3): 201-210.

[83] Kuhnert H, Kuhlmann H, Mohtadi M, et al. Holocene tropical western Indian Ocean sea surface temperatures in covariation with climatic changes in the Indonesian region [J]. Paleoceanography, 2014, 29(5): 423-437.

[84] Romahn S, Mackensen A, Groeneveld J, et al. Deglacial intermediate water reorganization: new evidence from the Indian Ocean [J]. Climate of the Past, 2014, 10(1): 293-303.

[85] Wang Y V, Leduc G, Regenberg M, et al. Northern and southern hemisphere controls on seasonal sea surface temperatures in the Indian Ocean during the last deglaciation [J]. Paleoceanography, 2013, 28(4): 619-632.

[86] Govil P, Naidu P D. Evaporation - precipitation changes in the eastern Arabian Sea for the last 68 ka: Implications on monsoon variability [J]. Paleoceanography, 2010, 25(1): PA1210.

[87] Kiefer T, McCave I N, Elderfield H. Antarctic control on tropical Indian Ocean sea surface temperature and hydrography [J]. Geophysical Research Letters, 2006, 33(24): L24612.

[88] Weldeab S, Lea D W, Oberhänsli H, et al. Links between southwestern tropical Indian Ocean SST and precipitation over southeastern Africa over the last 17 kyr [J]. Palaeogeography, Palaeoclimatology, Palaeoecology, 2014, 410: 200-212.

[89] Clemens S C, Yamamoto M, Thirumalai K, et al. Remote and local drivers of Pleistocene South Asian summer monsoon precipitation: a test for future predictions [J]. Science Advances, 2021, 7(23): eabg3848.

[90] Pei R J, Kuhnt W, Holbourn A, et al. Evolution of sea surface hydrology along the Western Australian margin over the past 450 kyr [J]. Paleoceanography and Paleoclimatology, 2021, 36(11): e2021PA004222.

[91] Yang Y P, Xiang R, Huang Y, et al. Meridional migration of Indian Ocean Monsoon precipitation during the early Holocene: evidence from the Andaman Sea [J]. Quaternary Science Reviews, 2021, 267: 107102.

[92] Liu S F, Ye W X, Chen M T, et al. Millennial-scale variability of Indian summer monsoon during the last 42 kyr: evidence based on foraminiferal Mg/Ca and oxygen isotope records from the central Bay of Bengal [J]. Palaeogeography, Palaeoclimatology, Palaeoecology, 2021, 562: 110112.

[93] Nürnberg D, Ziegler M, Karas C, et al. Interacting Loop Current variability and Mississippi River discharge over the past 400 kyr [J]. Earth and Planetary Science Letters, 2008, 272(1-2): 278-289.

[94] Schmidt M W, Lynch - Stieglitz J. Florida Straits deglacial temperature and salinity change: implications for tropical hydrologic cycle variability during the Younger Dryas [J]. Paleoceanography, 2011, 26(4): PA4205.

[95] Antonarakou A, Kontakiotis G, Mortyn P G, et al. Biotic and geochemical ($\delta^{18}O$, $\delta^{13}C$, Mg/Ca, Ba/Ca) responses of *Globigerinoides ruber* morphotypes to upper water column variations during the last deglaciation, Gulf of Mexico [J]. Geochimica et Cosmochimica Acta, 2015, 170: 69-93.

[96] Flower B P, Hastings D W, Hill H W, et al. Phasing of deglacial warming and Laurentide Ice Sheet meltwater in the Gulf of Mexico [J]. Geology, 2004, 32(7): 597-600.

[97] Zarriess M, Johnstone H, Prange M, et al. Bipolar seesaw in the northeastern tropical Atlantic during Heinrich stadials [J]. Geophysical Research Letters, 2011, 38(4): L04706.

[98] Zarriess M, Mackensen A. The tropical rainbelt and productivity changes off northwest Africa: a 31, 000-year high-resolution record [J]. Marine Micropaleontology, 2010, 76(3-4): 76-91.

[99] Weldeab S, Schneider R R, Kölling M, et al. Holocene African droughts relate to eastern equatorial Atlantic cooling [J]. Geology, 2005, 33(12): 981-984.

[100] Arbuszewski J A, Demenocal P B, Cléroux C, et al. Meridional shifts of the Atlantic intertropical convergence zone since the Last Glacial Maximum [J]. Nature Geoscience, 2013, 6(11): 959-962.

[101] Reißig S, Nürnberg D, Bahr A, et al. Southward displacement of the North Atlantic subtropical gyre circulation system during North Atlantic cold spells [J]. Paleoceanography and Paleoclimatology, 2019, 34(5): 866-885.

[102] Lin H L, Peterson L C, Overpeck J T, et al. Late Quaternary climate

change from $\delta^{18}O$ records of multiple species of planktonic foraminifera: high - resolution records from the Anoxic Cariaco Basin, Venezuela [J]. Paleoceanography, 1997, 12(3): 415-427.

[103] Lea D W, Pak D K, Peterson L C, et al. Synchroneity of tropical and high-latitude Atlantic temperatures over the last glacial termination [J]. Science, 2003, 301(5638): 1361-1364.

[104] Weldeab S, Schneider R R, Kölling M. Deglacial sea surface temperature and salinity increase in the western tropical Atlantic in synchrony with high latitude climate instabilities [J]. Earth and Planetary Science Letters, 2006, 241(3-4): 699-706.

[105] Santos T P, Lessa D O, Venancio I M, et al. Prolonged warming of the Brazil Current precedes deglaciations [J]. Earth and Planetary Science Letters, 2017, 463: 1-12.

[106] Lessa D V O, Venancio I M, dos Santos T P, et al. Holocene oscillations of Southwest Atlantic shelf circulation based on planktonic foraminifera from an upwelling system (off Cabo Frio, Southeastern Brazil) [J]. The Holocene, 2016, 26(8): 1175-1187.

[107] Hoffmann J, Bahr A, Voigt S, et al. Disentangling abrupt deglacial hydrological changes in northern South America: insolation versus oceanic forcing [J]. Geology, 2014, 42(7): 579-582.

[108] Schmidt M W, Weinlein W A, Marcantonio F, et al. Solar forcing of Florida Straits surface salinity during the early Holocene [J]. Paleoceanography, 2012, 27(3): PA3204.

[109] Parker A O, Schmidt M W, Jobe Z R, et al. A new perspective on West African hydroclimate during the last deglaciation [J]. Earth and Planetary Science Letters, 2016, 449: 79-88.

[110] Bemis B E, Spero H J, Bijma J, et al. Reevaluation of the oxygen isotopic composition of planktonic foraminifera: experimental results and revised paleotemperature equations [J]. Paleoceanography, 1998, 13(2): 150-160.

[111] Mulitza S, Boltovskoy D, Donner B, et al. Temperature: $\delta^{18}O$ relationships of planktonic foraminifera collected from surface waters [J]. Palaeogeography, Palaeoclimatology, Palaeoecology, 2003, 202(1-2): 143-152.

[112] Lambeck K, Rouby H, Purcell A, et al. Sea level and global ice volumes from the Last Glacial Maximum to the Holocene [J]. Proceedings of the National Academy of Sciences of the United States of America, 2014, 111(43): 15296-15303.

[113] Schrag D P, Adkins J F, McIntyre K, et al. The oxygen isotopic composition of seawater during the Last Glacial Maximum [J]. Quaternary Science Reviews, 2002, 21(1-3): 331-342.

[114] LeGrande A N, Schmidt G A. Global gridded data set of the oxygen isotopic composition in seawater [J]. Geophysical Research Letters, 2006, 33(12): L12604.

[115] Manabe S, Stouffer R J. Two stable equilibria of a coupled ocean-atmosphere model [J]. Journal of Climate, 1988, 1(9): 841-866.

[116] Zaucker F, Broecker W S. The influence of atmospheric moisture transport on the fresh water balance of the Atlantic drainage basin: general circulation model simulations and observations [J]. Journal of Geophysical Research:Atmospheres, 1992, 97(D3): 2765-2773.

[117] Joussaume S, Sadourny R, Vignal C. Origin of precipitating water in a numerical simulation of the July climate [J]. Ocean-Air Interactions, 1986, 1(1): 43-56.

[118] Schmittner A, Clement A C. Sensitivity of the thermohaline circulation to tropical and high latitude freshwater forcing during the last glacial - interglacial cycle [J]. Paleoceanography, 2002, 17(2): 1017.

[119] Broecker W S, Blanton S, Smethie Jr W M, et al. Radiocarbon decay and oxygen utilization in the deep Atlantic Ocean [J]. Global Biogeochemical Cycles, 1991, 5(1): 87-117.

[120] Carlson A E, LeGrande A N, Oppo D W, et al. Rapid early Holocene deglaciation of the Laurentide ice sheet [J]. Nature Geoscience, 2008, 1(9): 620-624.

[121] Ullman D J, Carlson A E, Hostetler S W, et al. Final Laurentide ice-sheet deglaciation and Holocene climate-sea level change [J]. Quaternary Science Reviews, 2016, 152: 49-59.

[122] Bentley M J. The Antarctic palaeo record and its role in improving predictions of future Antarctic Ice Sheet change [J]. Journal of Quaternary Science, 2010, 25(1): 5-18.

[123] Moy C M, Seltzer G O, Rodbell D T, et al. Variability of El Niño/Southern Oscillation activity at millennial timescales during the Holocene epoch [J]. Nature, 2002, 420(6912): 162-165.

[124] Conroy J L, Overpeck J T, Cole J E, et al. Holocene changes in eastern tropical Pacific climate inferred from a Galápagos lake sediment record [J]. Quaternary Science Reviews, 2008, 27(11-12): 1166-1180.

[125] Liu Z Y, Lu Z Y, Wen X Y, et al. Evolution and forcing mechanisms of El Niño over the past 21, 000 years [J]. Nature, 2014, 515(7528): 550-553.

[126] Partin J W, Cobb K M, Adkins J F, et al. Millennial-scale trends in west Pacific warm pool hydrology since the Last Glacial Maximum [J]. Nature, 2007, 449(7161): 452-455.

[127] Weber M E, Lantzsch H, Dekens P, et al. 200, 000 years of monsoonal history recorded on the lower Bengal Fan-strong response to insolation forcing [J]. Global and Planetary Change, 2018, 166: 107-119.